Journal of
Composites Science

MDPI

Article

Static Fatigue of SiC/SiC Minicomposites at High Temperatures Up to 1200 °C in Air: Multiscale Approach

Jacques Lamon [1,*] and Adrien Laforêt [2]

[1] LMT-Ecole Normale Supérieure Paris-Saclay, 75005 Cachan, France
[2] MONTUPET, 60290 Laigneville, France; adrien.laforet@montupet-group.fr
* Correspondence: Jacques.lamon@ens-paris-saclay.fr

Abstract: The present paper investigates the static fatigue behavior of Hi-Nicalon fiber-reinforced SiC–SiC minicomposites at high temperatures in the 900–1200 °C range, and under tensile stresses above the proportional limit. The stress–rupture time relation was analyzed with respect to subcritical crack growth in filaments and fiber tow fracture. Slow crack growth from flaws located at the surface of filaments is driven by the oxidation of free carbon at the grain boundaries. Lifetime of the reinforcing tows depends on the statistical distribution of filament strength and on structural factors, which are enhanced by temperature increase. The rupture time data were plotted in terms of initial stresses on reinforcing filaments. The effect of temperature and load on the stress–rupture time relation for minicomposites was investigated using results of fractography and predictions of minicomposite lifetime using a model of subcritical growth for critical filaments. The critical filament is the one whose failure by slow crack-growth triggers unstable fracture of the minicomposite. This is identified by the strength–probability relation provided by the cumulative distribution function for filament strength at room temperature. The results were compared to the fatigue behavior of dry tows. The influence of various factors related to oxidation, including multiple failures, load sharing, and variability, was analyzed.

Keywords: fiber; tow; minicomposite; lifetime; static fatigue; slow crack growth; fracture probability

Citation: Lamon, J.; Laforêt, A. Static Fatigue of SiC/SiC Minicomposites at High Temperatures Up to 1200 °C in Air: Multiscale Approach. *J. Compos. Sci.* **2021**, *5*, 67. https://doi.org/10.3390/jcs5030067

Academic Editor: Francesco Tornabene

Received: 22 January 2021
Accepted: 23 February 2021
Published: 28 February 2021

1. Introduction

Continuous fiber reinforced ceramic matrix composites (CMCs) exhibit a combination of superior properties over monolithic ceramics that make them attractive for high temperature applications. This results from the fiber reinforcement that induces composite damage tolerance, and which implies significant performance, such as high resistance to fatigue, creep, and fracture, and high reliability. Furthermore, the CMCs are endowed with a remarkable versatility, which means that the behavior of CMCs can be designed with respect to expected performances, through the selection of fiber and matrix types with appropriate properties. This multiscale scheme is illustrated in the present paper, which analyzes the static fatigue behavior of SiC/SiC minicomposites, with respect to the delayed failure of reinforcing filaments and tows.

CMCs like SiC/SiC, which consist of an SiC matrix reinforced by SiC fibers, exhibit high mechanical properties at high temperatures and in severe environments [1,2]. They were developed initially for military and aerospace applications. Now they are being introduced into new fields, such as stationary gas turbines for the co-generation of heat and power, and their range of applications will grow when their cost is lowered significantly. They are candidate materials for many high-temperature structural applications. Potential applications include heat exchangers, heat engines, gas turbines, structural components in aeronautical and aerospace industry, nuclear reactors, fusion power reactors, etc. Thus, controlling and predicting the rupture time of CMCs under fatigue conditions has become an important issue, with a view to long-term applications.

Most of the papers in the literature on the high temperature behavior of fibers and CMCs first examined the creep behavior under a constant load (at temperatures > 1200 °C), and the strength degradation of unstressed fibers by heat treatment or oxidation (at temperatures > 1000 °C). Strength degradation of fibers has been attributed to various phenomena, including flaw size increase, nucleation of new flaws, formation of a silica layer on the surface of fibers, and grain growth [3–11]. Lara-Curzio [9,10] modelled the stress–rupture time behavior of stressed fiber bundles and composites, delayed failure being attributed to the formation of a silica layer on the fiber surface that results in loss of fiber strength. Parthasarathy et al. [11] also postulated that the loss in fiber strength is predictable by considering the scale thickness as a strength-limiting flaw. DiCarlo et al. [4,8,12,13] compared the strength dependence to time, temperature, and size for a variety of oxide and SiC-based fibers using a phenomenological approach based on empirical Larson–Miller and Monkman–Grant rupture plots. Morscher compared the stressed oxidation lifetime properties of several SiC/SiC minicomposites, and used Larson–Miller plots to compare minicomposite and fiber data [14,15].

More recent papers have identified the fundamental process of delayed failure on stressed SiC-based single filaments, on multifilament tows, and on SiC/SiC, in air at temperatures in the intermediate range (between 500–800 °C) [16–18]. Delayed failure was found to result from the subcritical propagation of cracks in filaments, initiated from surface defects, as a result of the consumption of free carbon at grain boundaries and the local stresses induced by the SiC → SiO_2 transformation at the crack tip [16,17]. Both phenomena may contribute simultaneously (Nicalon fibers) or sequentially (Hi-Nicalon S and SA3 fibers, which contain a little free carbon not connected) [17]. The Hi Nicalon fiber is essentially made of ~10 nm β-SiC nano-grains and a free carbon network [17]. Furthermore, sensitivity to delayed failure was found to decrease with the amount of oxygen present in the environment [17].

In the upper range of temperatures (900–1200 °C) [19,20] slow crack growth from flaws still operates on filaments. As temperature increases, a thicker oxide layer coats the fibers so that structural effects related to the growth of oxide scale on filaments occur. The growth of oxide scale on the fiber surface fosters the formation of groups of bonded fibers that fail simultaneously, which weakens tows [20].

The power function

$$V = A\, K_I^{\,n} \tag{1}$$

has been shown to provide a sound foundation to modeling subcritical crack propagation in filaments for prediction of the stress–rupture time relation for the static fatigue of fiber tows. Based on the model of slow crack growth of filaments and tows, it was shown that the static fatigue behavior of SiC Hi Nicalon tows at high temperatures (up to 1200 °C) in air was dictated by the delayed failure of a critical filament [20,21]. The critical filament is that filament whose fracture triggers complete failure of the tow. It is characterized by its room temperature strength and the corresponding failure probability in the cumulative distribution function. It depends on loading mode and temperature. Under a constant load, when filaments remain independent as observed at relatively low temperature (500 °C), the critical filament is characterized by the strength value corresponding to the theoretical value of failure probability $\alpha_t = 0.11$ for Hi Nicalon fiber [21]. When temperature increases, the critical filament is characterized by a lower value of initial strength, which decreases down to that of the weakest filament in the tow.

Fracture of CMCs is dictated by the fracture of fibers. This generally occurs when the matrix no longer shares the load, because it is cracked and debonded from the fibers. Fiber tows have been shown to be an appropriate length scale in multidirectional composites. Therefore, an appropriate approach is to relate the failure of composites to that of fiber tows, and to that of the filaments that constitute the tows.

A single tow minicomposite is an interesting specimen geometry for investigating the in-situ behavior of composite constituents, and for establishing models of behavior that involve microstructure–property relations. Furthermore, it constitutes an intermediate

length scale for woven composites. It has been used for investigating behavior at room temperature, using experimental and modeling approaches [22].

The present paper proposes a multiscale approach to the static fatigue of Hi Nicalon reinforced SiC/SiC minicomposites at high temperatures in air. The stress–rupture time diagrams were analyzed with respect to the delayed failure of reinforcing filaments and tows, using fractography and predictions of lifetime using a critical filament-based model of tow-delayed failure.

2. Theory: Static Fatigue of Filaments and Tows. The Concept of Critical Filament

2.1. Static Fatigue of Single Filaments under Constant Stress

The subcritical crack growth model is based on the following expansion of Equation (1), which is usually employed to describe the slow propagation of cracks caused by an environment under load in ceramics and glass materials [23–25]:

$$V = \frac{da}{dt} = V^* \left(\frac{K_I}{K_{IC}} \right)^n \tag{2}$$

where V is crack velocity, a is crack length, t is time, K_I is the stress intensity factor, K_{IC} is the critical stress intensity factor, and V^* and n are constants depending, respectively, on environment and material. The environment dependence of V^* is assumed to be defined by the Arrhenius law:

$$V^*(T) = V_0^* exp\left(-\frac{E_a}{RT} \right) \tag{3}$$

where T is temperature, $V_0{}^*$ is the temperature independent material parameter, E_a is activation energy, and $R = 8.314$ J K^{-1} mol^{-1}.

During a time period (t_F) under constant stress (σ) on a filament, a crack propagates from initial flaw size (a_i) to length (a_R), and the stress intensity factor increases from K_{Ii} to K_{IR}. The filament strength decreases. The residual strength (σ_R) at time (t_F) is (Appendix A):

$$\sigma_R^{n-2} = \sigma_f^{n-2} - t_F \frac{V^* \sigma^n Y^2 (n-2)}{2K_{IC}^2} \tag{4}$$

where σ_f is the initial strength of the filament. Failure of filament occurs when residual strength (σ_R) has decreased to the stress on the filament (σ). Filament lifetime is derived from Equation (4) for $\sigma_R = \sigma$:

$$t = \frac{2K_{IC}^2}{V^* Y^2 \sigma^2 (n-2)} \left[\left(\frac{\sigma_f}{\sigma} \right)^{n-2} - 1 \right] \tag{5}$$

The bundle model [24,26,27] describes the behavior of a population of parallel, independent, and identical filaments under a tensile load. Filament strengths display wide variability as a result of the random distribution of fracture inducing flaws. The statistical distribution of filament initial strengths (σ_f) is generally characterized by the Weibull cumulative distribution function:

$$P = 1 - exp\left[-\frac{v}{v_0} \left(\frac{\sigma_f}{\sigma_0} \right)^m \right] \tag{6}$$

where P is failure probability, m and σ_0 are statistical parameters, v is the volume of a single filament, and v_0 is reference volume ($v_0 = 1$ m^3 in the present paper).

Strength data are ordered from smallest to largest, the reference strength of the j^{th} filament with failure probability P_j is derived from Equation (6):

$$\sigma_{fj} = \sigma_0 \left(-\frac{v_0}{v} Ln(1 - P_j) \right)^{\frac{1}{m}} \tag{7}$$

A filament in a tow is identified by the initial strength, as well as by the corresponding value of cumulative probability, according to Equations (6) and (7). As a consequence of filament strength variability, residual strength and lifetime are random variables according to relations (4) and (5). The strength–probability–time relation for filaments is derived from the combination of Equations (5) and (7) [21]:

$$P(t,\sigma,v) = 1 - exp\left[-\left(\frac{v}{v_0}\right)\left(\frac{\sigma}{\sigma_0}\right)^m\left(1+\frac{t}{t^*}\frac{n-2}{2}\right)^{\frac{m}{n-2}}\right] \quad (8)$$

where $P(t, \sigma, v)$ is the failure probability at time t, under constant stress σ, for a filament with volume v. t^* this is a stress dependent scale factor: $t^* = \frac{K_{IC}^2}{V^*\sigma^2Y^2}$

2.2. Lifetime of Fiber Tows under Constant Force

2.2.1. Equal Load Sharing

A filament in a tow breaks when $\sigma_R < \sigma$, whereas those filaments having $\sigma_R > \sigma$ survive and carry equally the constant applied load. According to Equation (9), under a constant force σ increases when a filament fails:

$$\sigma = \frac{F}{N_0 S_f(1 - N/N_0)} = \frac{\sigma_a}{1 - N/N_0} \quad (9)$$

where N is the number of broken filaments, and S_f is the filament cross sectional area. $\sigma_a = F/N_0S_f$ is the initially applied stress on the tow. When the filaments fail one after one, $N = j$ at failure of the j^{th} filament; by contrast, when groups of filaments fail, $N > j$.

The particular filament that triggers catastrophic failure of a tow is referred to as the critical filament. Under constant force and global load sharing this filament exhibits the longest lifetime. When filaments fail one after one, according to an ascending order of strengths ($N = j$), $\alpha = N/N_0$ is the value of the cumulative probability P for the N^{th} filament. It defines the N^{th} filament throughout its whole life. The critical filament is defined by the following particular value of probability (α) that is derived from the maximum of function $t(\sigma_f(p))$ (Equation (8) for σ given by Equation (9)) [21]:

$$P = \alpha_t = 1 - exp\left(-\frac{n-2}{nm}\right) \quad (10)$$

Figure 1 shows the distribution of filament lifetimes calculated when filaments fail one after one, using the following equations [21]: Equation (5) for lifetime, and Equation (7) for filament strength. Characteristics of filaments and tows are given in Table 1. Figure 1 shows that the maximum lifetime was obtained for $P = \alpha_t$ (= 0.11 for Hi Nicalon fiber). This agrees with the prediction by Equation (10).

When groups of filaments fail together ($N > j$), a closed-form expression for $t(\sigma_f(P))$ is not available, since the size of the groups of filaments is unpredictable. A distribution of lifetimes $t(\sigma_f(P))$ can be calculated stepwise considering arbitrary sizes of groups of failures. Figure 1 shows various examples of distributions of filament lifetimes calculated for arbitrary sizes of groups of filaments [21]. Lower values of maximum lifetimes and of α_t were obtained when it was supposed that the failure of groups of filaments was concomitant with the failure of a filament from slow crack growth. The filament lifetime decrease beyond $P = \alpha_t$ results from the increase of stress on a filament relative to filament strength.

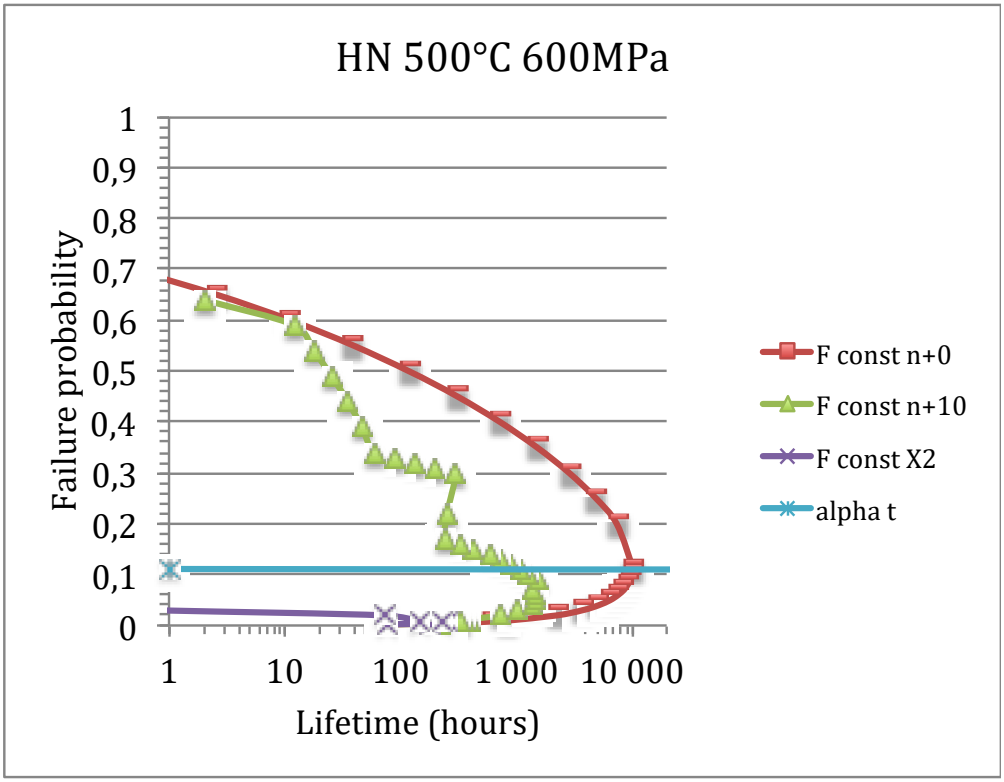

Figure 1. Predicted statistical distributions of lifetimes at 500 °C under constant force (initial stress on filaments 600 MPa) and equal load sharing for Hi Nicalon filaments of a tow: $n + 0$ stands for failure one after another, $n + 10$ for failure of groups of 10 filaments, and X2 for failures of groups of filaments with size doubled at each step. Additionally indicated is the failure probability ($\alpha_t = 0.11$) of critical filament. Failure probability defines a filament with respect to the cumulative distribution function for strengths [21].

Table 1. Hi Nicalon filament and tow characteristics.

Filaments	Hi-Nicalon	Reference
Young's modulus: E_f (GPa)	280	[19]
Filament radius: r_f (μm)	7	
Gauge length: l_0 (mm)	25	
K_{IC} (MPa$\sqrt{}$m)	1.7	[21]
Y	1.12	
n	12.6	[24]
V_0* (m/s)	40.5	[24]
V* (m/s) 500 °C	4.98×10^{-9}	[24]
V* (m/s) 800 °C	2.96×10^{-6}	[24]
V* (m/s) 900 °C	1.15×10^{-5}	
V* (m/s) 1000 °C	3.76×10^{-5}	
V* (m/s) 1200 °C	2.48×10^{-4}	
Activation energy (kJ/mol)	146.7	[24]
m	6.8	[16]
σ_0 (MPa)	61	[16]
Reference volume: v_0 (m^3)	1	
Tows		
Number of filaments: N_0	500	

2.2.2. Local Load Sharing

In local load sharing conditions in the presence of N broken filaments, the load that was carried by the new j filaments that failed is then shared locally by a few neighboring filaments (k filaments). Thus, these k filaments carry the force:

$$F = \frac{F_a}{N_0 - N} + j\frac{F_a}{k(N_0 - N)} \quad (11)$$

The stress on the k reloaded filaments is then:

$$\sigma_{jk} = \frac{F}{S_f} = (\frac{j}{k} + 1)\frac{\sigma_a N_0}{k(N_0 - N)} \quad (12)$$

3. Experimental Procedure

A minicomposite is a composite reinforced by a single fiber tow. The SiC/SiC minicomposites in this paper consisted of an SiC matrix and Pyrocarbon (PyC) interphase, produced by CVI on unidirectional preforms of SiC Hi-Nicalon fiber tows. Hi Nicalon tow contains 500 filaments, each of 15-micrometer average diameter.

3.1. Static Fatigue Tests on Minicomposites

Minicomposite ends were affixed within alumina tubes using alumina-based cement (Figure 2). The upper tube was gripped by the testing machine, and a dead-weight-load was hung gradually from the lower tube (this operation took <10 s) (Figure 2). The gauge length (25 mm) was located in the furnace hot-zone at uniform temperature (hot grip technique). The gauge length is defined as the inner distance between the alumina tubes. A silica tube protected the specimen against possible pollution from furnace elements, and allowed environmental control through a constant gas flow (N_2/O_2). The test specimens were heated up to the test temperature before loading (heating rate ~20 °C/min). Lifetime was captured automatically by a computer when the specimen failed. Much care was taken during test specimen preparation and handling. The template used to ensure alignment of minicomposites within the alumina tubes is shown on Figure 2. Rotating upper and lower linkage systems allowed alignment of the test specimen.

The fractured specimens were examined using scanning electron microscopy.

3.2. Tensile Behavior of Minicomposites at Room Temperature

Monotonous tensile tests on minicomposite specimens were conducted at room temperature in order to determine the stresses operating on filaments in minicomposites during static fatigue under constant force. The force–strain behavior of minicomposites was compared to that of a dry tow. A standardized testing procedure was applied for the tensile tests on dry tows [28]. This technique was also applied to minicomposites. Test specimens with 25, 50, and 75 mm gauge lengths were prepared. Specimen ends were glued within 40-mm length metallic tubes, which were then gripped by the testing machine. A device was designed to achieve the perfect alignment of specimens. The specimens were loaded at a constant deformation rate (5 mm/min) on a tensile machine at room temperature. The loading system compliance (C_s) was measured using specimens having decreasing gauge lengths (C_s = 2.55 10^{-4} mm/N) [19].

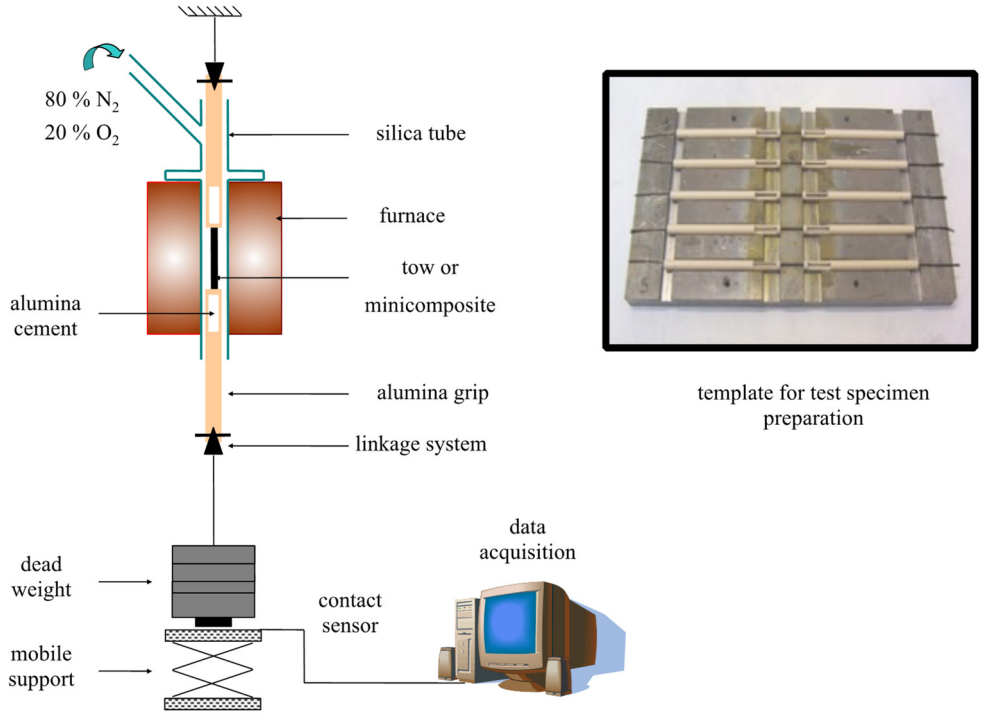

Figure 2. Machine for static fatigue testing of multifilament tows and minicomposites at high temperature. Additionally shown is the template used for specimen preparation and alignment of minicomposites within the alumina tubes.

4. Results

4.1. Tensile Behavior of Tows and Minicomposites

Figure 3 shows typical tensile behaviors for dry tows and minicomposites. The minicomposites exhibited non-linear deformations beyond the proportional limit (F_e = 70 N, Figure 3), which reflects transverse matrix cracking [22]. The dry tow exhibited non-linear deformations beyond the proportional limit (F_{te} = 120 N, Figure 3), which reflects individual fiber breaks.

Table 2 summarizes the main characteristics of minicomposites. It is worth noting that the elastic modulus coincides with the value predicted using the mixture law for E_m = 410 MPa, and E_f = 280 GPa. This indicates that all the filaments initially carried the load. This was expected owing to the fiber matrix bonding that allows load transfers in the presence of initially broken filaments. It can be noted that the tensile curves of dry tow and minicomposites are consistent since they meet close to maximum force. At this stage, the filaments carry the load while the cracked and debonded matrix does not share the load.

The force on the dry tow (F_{tow}) was determined graphically from F_{mini}, as shown in Figure 3. The stress on the fiber was calculated from F_{tow} using Equation (13):

$$\sigma = \frac{F_{tow}(\varepsilon)}{N_0 S_f} \tag{13}$$

where $F_{tow}(\varepsilon)$ denotes the force on filaments in tow at strain ε, S_f is the average cross-sectional area of filaments.

The load on minicomposite (F_{mini}) during static fatigue was selected such that corresponding F_{tow} was smaller than the tow elastic limit, to ensure that single filaments did not fail during application of the dead weight. F_{mini} was larger than minicomposite proportional limit (F_e) for most tests, so that the matrix contained matrix cracks at the beginning of static fatigue. Those specimens tested at $F_{mini} < F_e$ did not fail during static fatigue.

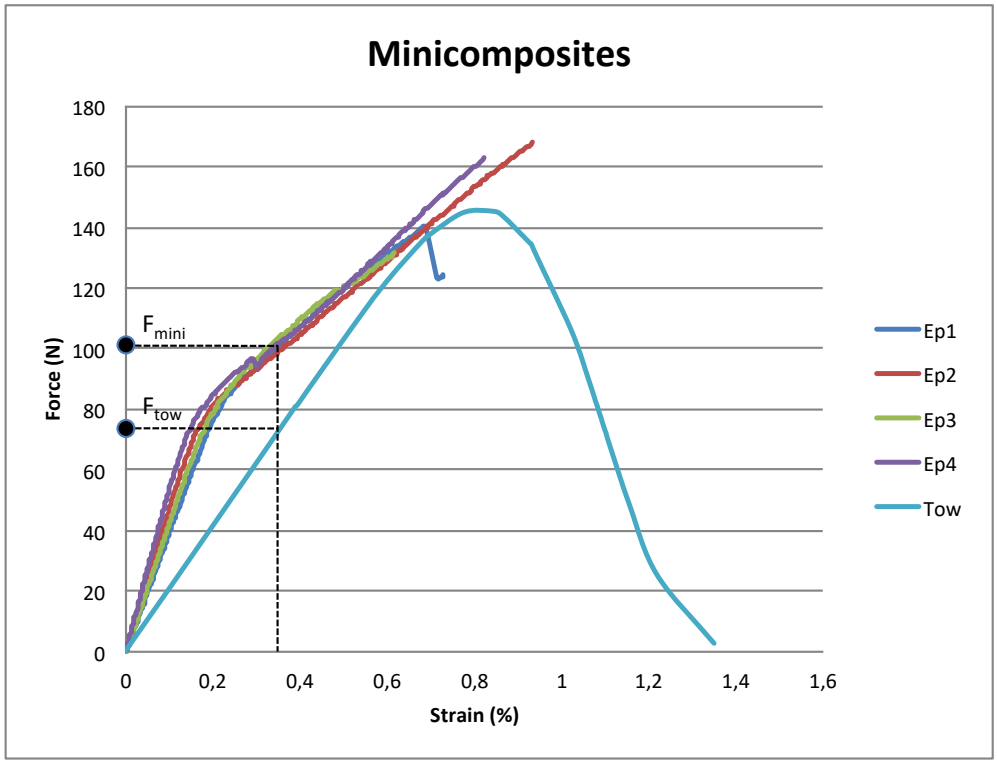

Figure 3. Tensile behavior of Hi Nicalon/SiC minicomposites at room temperature. Comparison with that of a Hi Nicalon fiber tow.

Table 2. Main characteristics and tensile behavior of Hi Nicalon/PyC/SiC minicomposites and dry tows [19].

Minicomposites		
Cross sectional area	S_{mini} (mm^2)	0.25
Fiber volume fraction	V_f (%)	29
Rupture force	F_R (N)	130–167
Strain-to-failure	ε_R(%)	0.48–0.76
Force at proportional limit	F_e (N)	58–73
Strain at	ε_e(%)	0.052–0.12
Young's modulus	E_{mini} (GPa)	362
Force at matrix cracking Saturation	F_{sat} (N)	98
Strain at matrix cracking Saturation	ε_{sat}(%)	0.28
Tows		
Number of filaments		500
Fiber Young's modulus	(GPa)	280
Tow force at proportional limit	F_{te} (N)	120
Tow strain at	ε_{te}(%)	0.58
Tow maximum force	F_t (N)	145
Tow strain at maximum force	ε_t(%)	0.8

4.2. Stress–Rupture Time Diagrams of Minicomposites

Rupture times were plotted as a function of the stresses operating on the filaments. The remote stress on fibers (denoted σ) was derived from the force on the minicomposite (F_{mini}) by comparing the force–strain behavior to that of a dry tow at room temperature.

The stress–rupture time diagrams for the Hi-Nicalon/PyC/SiC minicomposites show that rupture times decreased when the stress increased (Figures 4–6). The power law $t = A/\sigma^p$ provides an approximation of the trend (Table 3). The data display variation. The scatter in data was significant at 1200 °C, and the R^2 parameter displayed a very low value (Table 3).

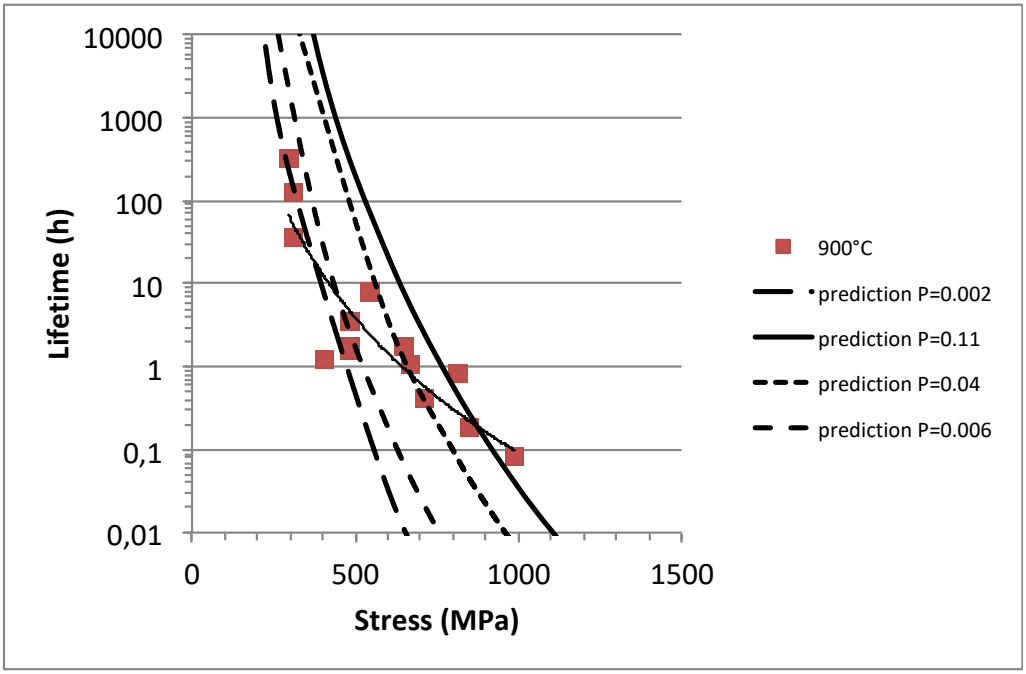

Figure 4. Static fatigue at 900 °C on minicomposites: comparison with stress–rupture time curves for critical filaments.

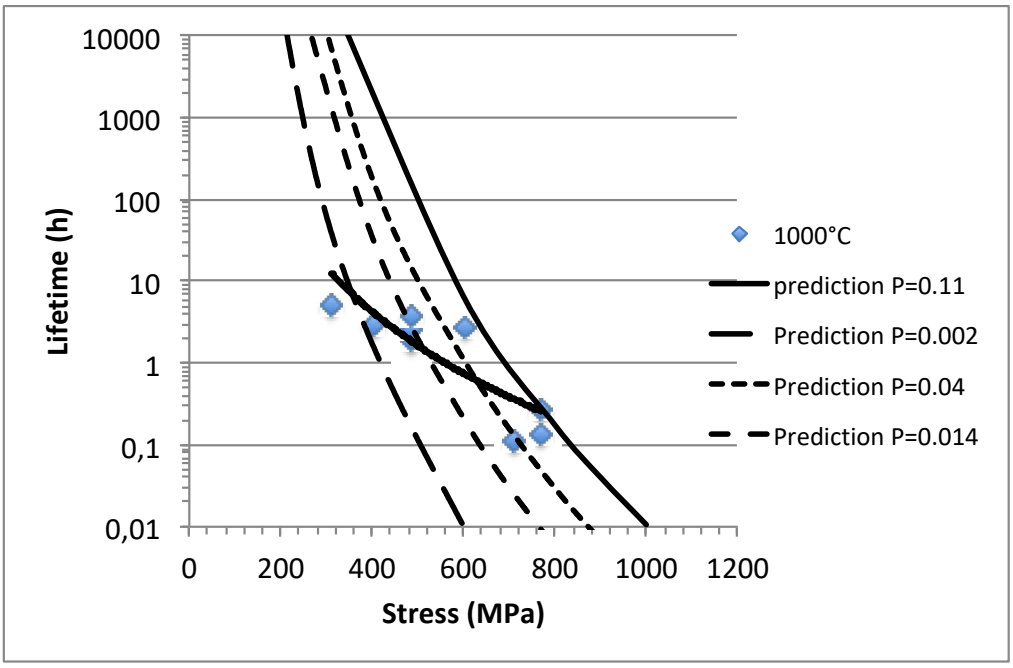

Figure 5. Static fatigue at 1000 °C on minicomposites: comparison with stress–rupture time curves for critical filaments.

Table 3. Estimates of stress exponent p and constant A at different temperatures for minicomposites.

Temperature	900 °C	1000 °C	1200 °C
p	5.4	4.3	3.8
A (sec.MPa^n)	6×10^{18}	2.5×10^{15}	3.5×10^{13}
R^2	0.8	0.7	0.09

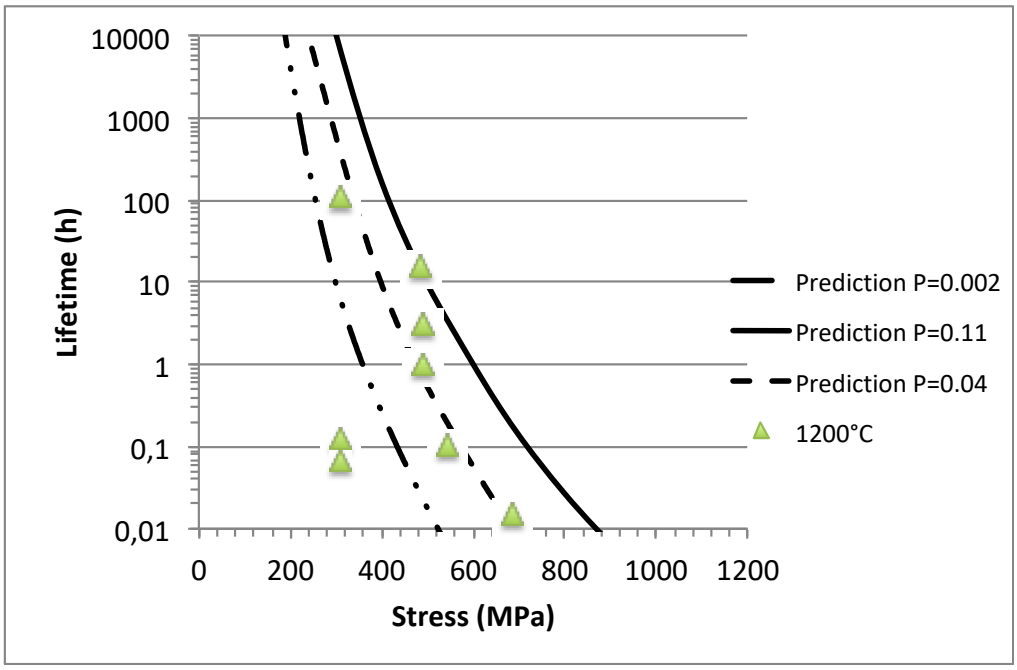

Figure 6. Static fatigue at 1200 °C on minicomposites: comparison with stress–rupture time curves for critical filaments.

The experimental stress–rupture time diagrams were compared to predictions for particular single filaments (Figures 4–6) obtained using Equations (5) and (7) for the following values of failure probability: (i) $P = 0.11 = \alpha_t$ given by Equation (10); (ii) $P = 0.002 = 1/500$ for the weakest filament; (iii) particular values of P that fit the data.

Figures 4–6 reveal variability in critical filament between $P = 0.002$ and $P = 0.11$. When $P = 0.11$, the failure mechanism is consistent with theory: the filaments failed individually one after another. This implies that the carbon fiber–matrix interface had been consumed due to the presence of matrix cracks. When $P = 0.002$, the weakest filament triggered fracture of all filaments as a result of strong interactions of filaments. When $0.002 < P < 0.12$ the failure process involved smaller groups of filaments.

The influence of temperature on the experimental stress–rupture time diagrams is not easily visible from Figures 4–6, owing to the scatter in data. The decrease of parameters P and A suggests that lifetime decreased with increasing temperature (Table 3). Figure 7 also shows that the bounds of the stress–rupture time diagrams ($P = 0.002$ and $P = 0.11$) decreased with increasing temperature. This suggests that the phenomenon of slow crack growth did not slow down when temperature increased, as could be expected when an oxidizing environment makes oxide scale grow on the filament surface.

4.3. Comparison with Dry Tows

The static fatigue behavior of Hi Nicalon fiber tows was investigated in previous papers [16,19–21]. The stress–rupture time diagrams were found to depend strongly on temperature, and to be affected by growth of the oxide scale at temperatures >900 °C. A comparison to those obtained on minicomposites at temperatures >900 °C (Figure 8) reveals significant differences, with weakening of dry tows at increasing temperatures. The superiority of minicomposites at stresses >300 MPa, can be attributed to the presence of the matrix.

At temperatures ≤800 °C, the growth of oxide scale was limited for the dry tows. The trend shown by the stress–rupture time diagram at 500 °C (Figure 9) is similar to that of minicomposites at 900 °C and 1000 °C (Figures 4 and 5). Most lifetimes were dictated by the critical filament defined by $P = \alpha_t = 0.11$, while a few data points at lower stresses and longer times were located close to the lower bound at $P = 0.002$ (Figure 9).

These latter lifetimes compared with predictions when groups of failures were considered (Figure 9) [21]. It can be conjectured that the longer time exposure made possible the growth of a significant oxide scale. As above, the experimental stress–rupture time data displayed variation (Figure 9), and were poorly fitted by the power law (Table 4).

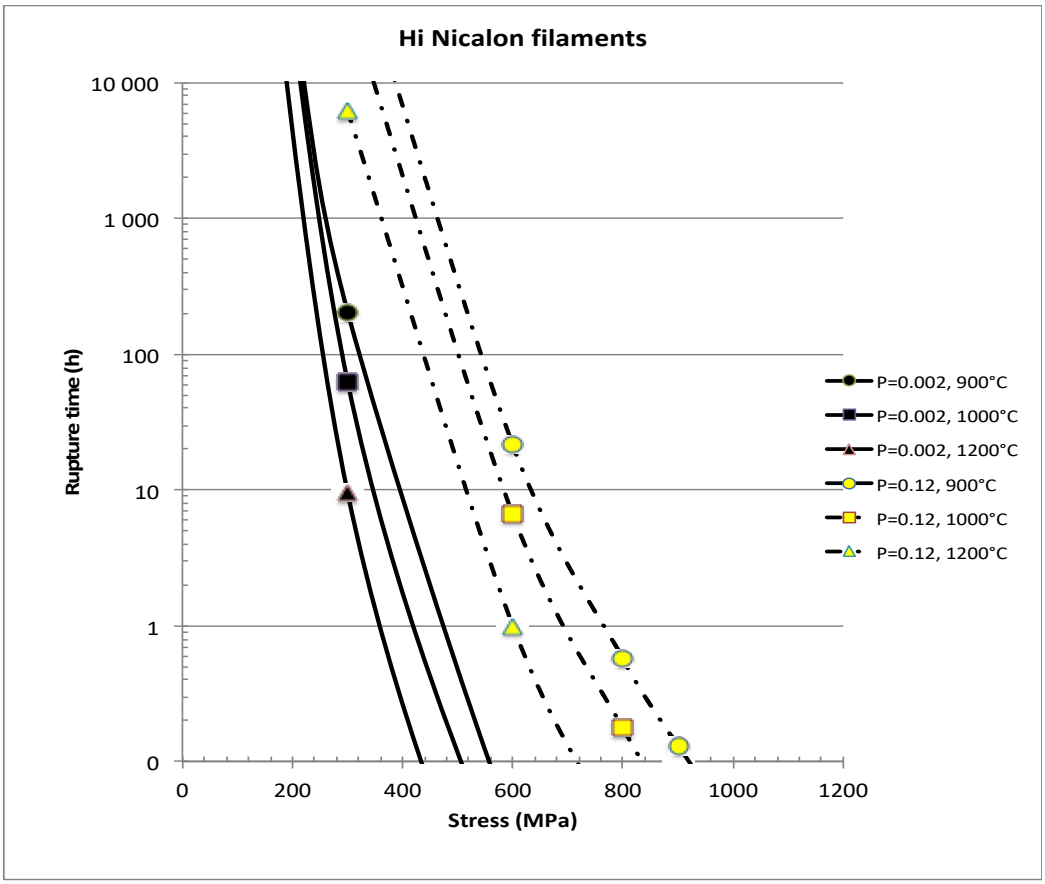

Figure 7. Influence of temperature on the lower and upper bounds of stress–rupture time diagrams for composites.

Table 4. Estimates of stress exponent p and constant A at temperatures for Hi Nicalon fiber tows [16,20].

Temperature	500 °C	800 °C	900 °C	1000 °C	1200 °C
p	8.45	8.34	13.4	27.3	31.4
A (sec.MPa^n)	1.05×10^{30}	3.36×10^{26}	2.42×10^{37}	1.13×10^{71}	9.08×10^{77}
R^2	0.73	0.76	0.58	0.53	0.9

At temperatures ≥900 °C [20], it was shown that the lifetimes of dry tows were dictated by the weakest filament (defined by $P = 0.002$). This behavior was shown to result from the rupture of groups of fibers stuck by the oxide scale grown on filaments. The lifetime of tows remained comparable to that predicted for the weakest filaments when temperature increased, which indicates that the phenomenon of slow crack growth was not slowed down by the growth of oxide scale. This result is at variance with earlier results of analysis based on the empirical stress–rupture time relation [19].

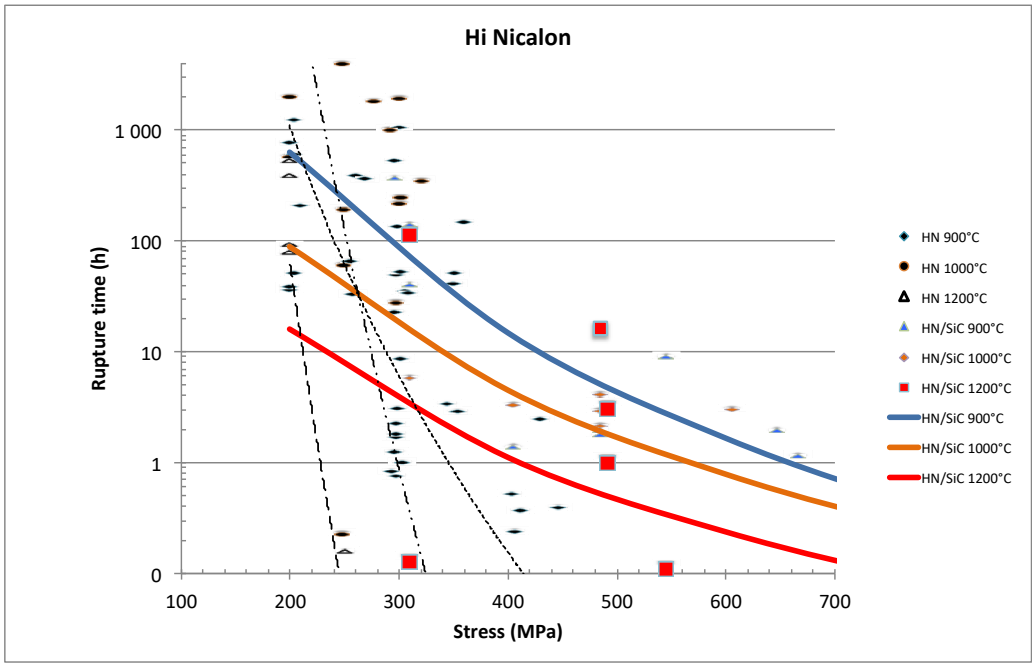

Figure 8. Comparison of static fatigue behavior of dry tows (- - - - - - -900 °C; —··—··—1000 °C; — — — — -1200 °C) and Hi Nicalon/SiC minicomposites at elevated temperatures >900 °C.

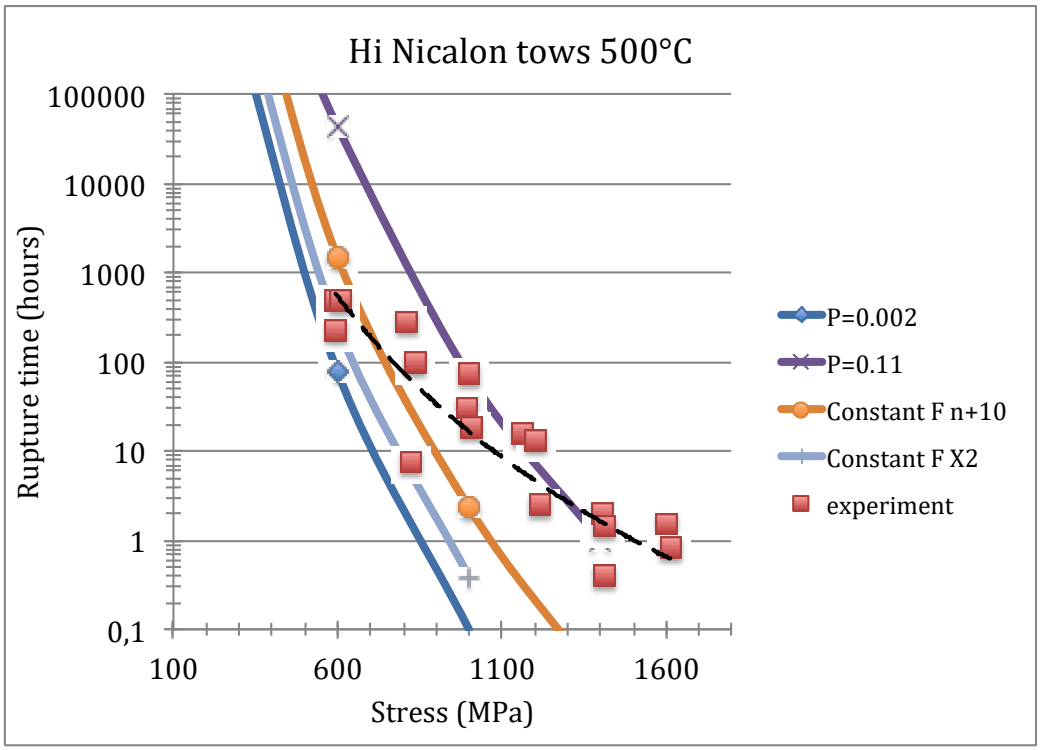

Figure 9. Static fatigue at 500 °C on SiC Hi Nicalon dry tows: comparison of experimental stress–rupture time diagram with predicted stress–rupture time curves for critical filaments (defined by failure probabilities $P = 0.002$, $P = 0.11$); and then considering failures of groups of 10 filaments ($n + 10$) or groups with sizes doubled at each step (X2) [21].

4.4. SEM Inspection of Minicomposites after Failure

After fatigue tests, the minicomposites were covered by an oxide layer. This layer was removed in a bath containing 40% fluoridic acid. This operation lasted 1 h. The fibers were not attacked by acid. Then, the fractured surface of the specimens was inspected by SEM. The following features were identified:

- Successive crack tips on the fracture surfaces of some filaments, which are typical of slow crack growth [17] (Figures 10 and 11).
- Mirrors on the fractured surface of some filaments that are indicative of catastrophic fracture from flaws inherent in the filaments. From this it can be inferred that the stress operating on the filaments was sufficiently high, and much higher than the stress applied during the fatigue test (Figure 11).
- Smooth filament fracture surfaces indicative of catastrophic fracture initiated outside the fiber (Figure 12).
- Clusters of fractured filaments (Figures 12 and 13).
- Debonded fiber–matrix interfaces at temperatures $\geq$900 °C (Figures 11 and 12).
- Oxide filling some fiber–matrix interfaces in place of the initial PyC interphase (Figure 13), or coating the filament and the matrix after tests at 1200 °C (Figure 13). The oxide layers at interface depended on the location of the filament within the minicomposite. The minicomposites tested at 1200 °C contained both debonded fibers, which are visible in Figure 14 as pulled out filaments, and filaments bonded to the matrix by oxide (Figures 13 and 14).

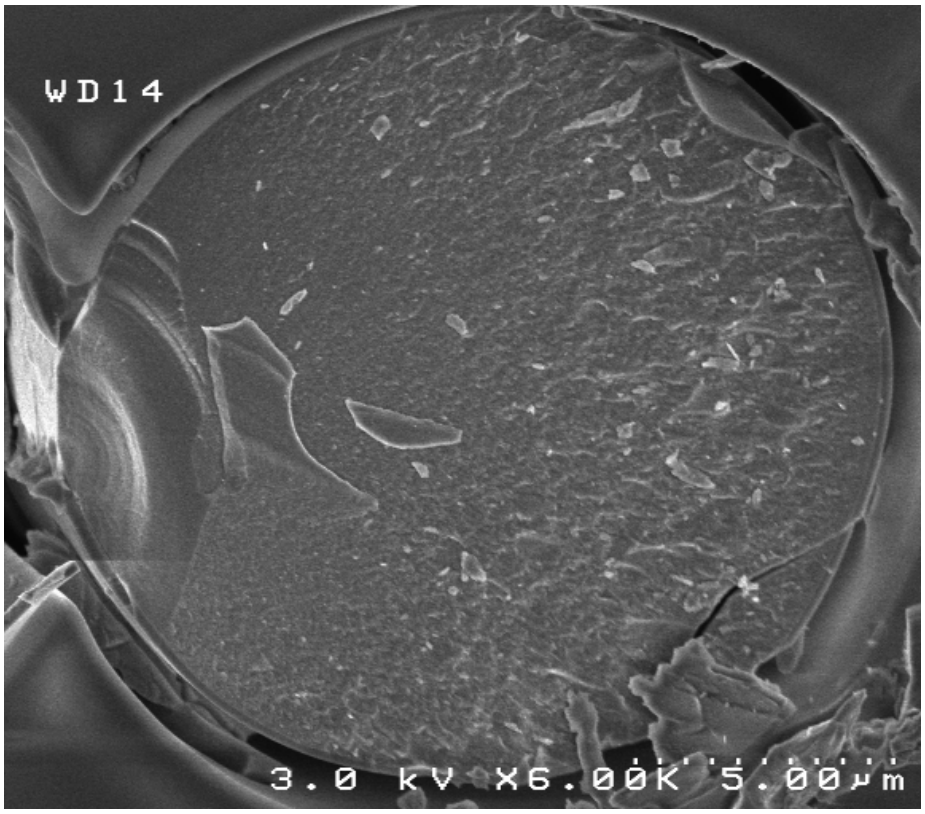

Figure 10. Typical facies of slow crack growth.

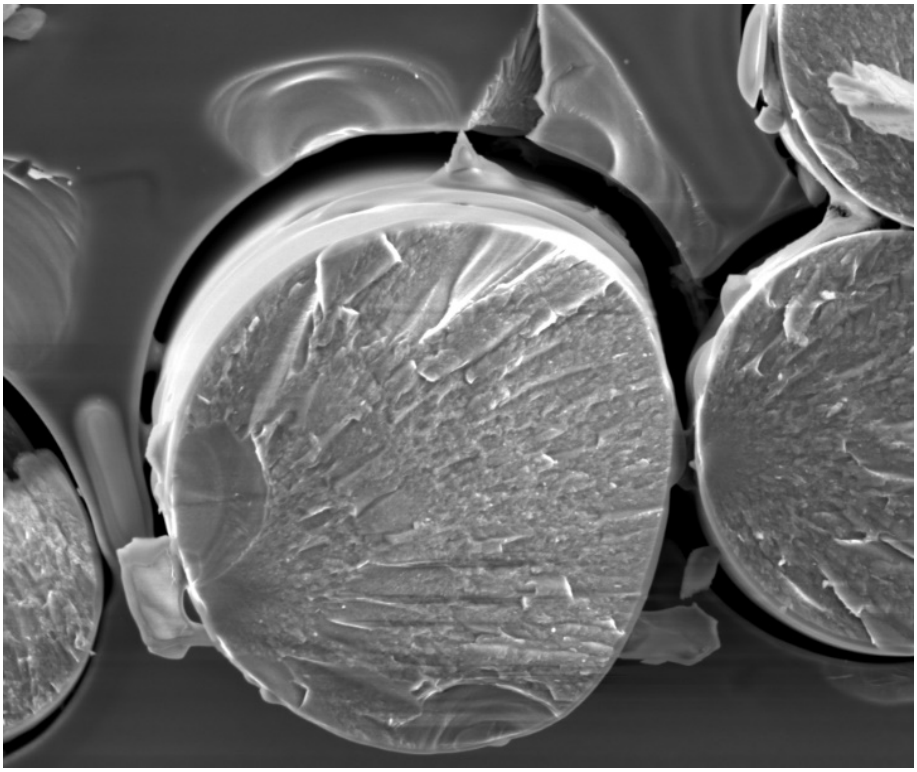

Figure 11. Typical facies of slow crack growth (on the left) and fracture mirror (on the right) after static fatigue at 900 °C. Note that the fibers are debonded (filament diameter = 14 micrometers).

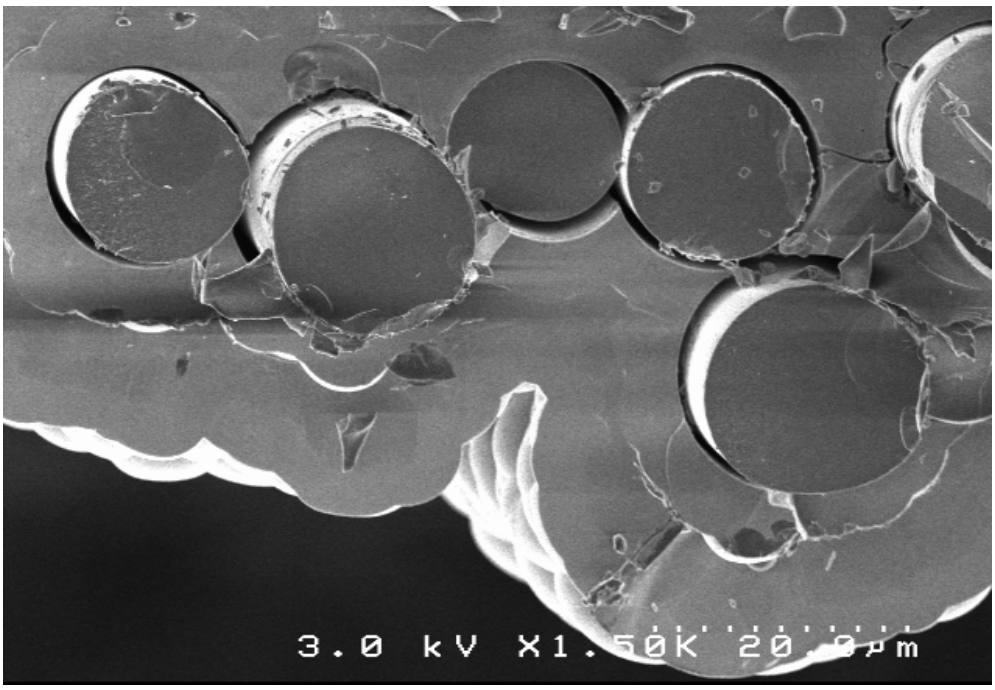

Figure 12. Example of group of filaments, with a smooth fracture surface close to the filament on the left, and with typical marks of slow crack growth. Note that the PyC interphase had disappeared.

Figure 13. Filaments bonded together, or bonded to the matrix by oxide in a minicomposite tested at 1200 °C.

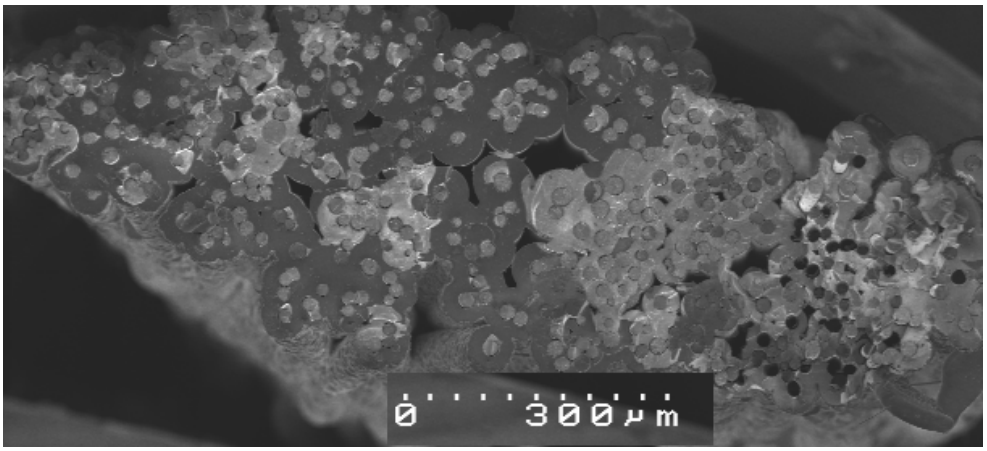

Figure 14. Minicomposite fractured surface after fatigue at 1200 °C, 525 MPa for 16 h.

4.5. Fracture Mechanism of Minicomposites

From the features identified by fractography, it can be inferred that the mechanism of delayed failure of minicomposites involved the combination of the following basic mechanisms:

(1) In the presence of matrix cracks, the pyrocarbon interphases are consumed, so that the filaments are exposed to oxidizing atmosphere, and carry the load.
(2) The filaments are subject to slow crack growth, activated by environment. The weakest filaments fail first, as the lifetime and residual strength of filaments are commensurate with filament strength/failure probabilities in the cumulative distribution function (Figure 1). The failures should follow a sequence dictated by the ascending order of strengths.

(3) These primary failures trigger the premature failure of neighboring filaments by overstressing (fracture mirrors) or by contact (filament clusters). These collateral fractures may eliminate any filament, strong as well as weak filaments, or potential critical filaments. As a consequence, the critical filament is affected, as shown earlier in Figure 1, and the minicomposite is weakened. The scatter in the fraction of collateral fractures and filaments broken by slow crack growth is a source of variability in lifetimes.

Figure 14 shows the fracture surface of a minicomposite specimen tested at 1200 °C. The filament fracture surfaces located in the matrix crack plane indicates catastrophic fracture. The 17 pulled out single filaments (most of them being indicated by black holes) failed, probably by slow crack growth. Among the extracted filaments three groups of two or three filaments can also be noticed. Therefore it can be inferred that around 20 failures by slow crack growth occurred. This represents 4% of the filaments in the minicomposite. This result compares with the trend shown in Figure 6, where some experimental data were predicted for a critical filament characterized by a probability of 0.04 in the cumulative distribution function.

4.5.1. Fracture Mirrors

Twenty one fracture mirrors were detected on a minicomposite specimen after a 3 h test at 900 °C, 525 MPa. Flaw strengths were derived from mirror sizes using the following equation:

$$\sigma_{mirror} = \frac{A}{\sqrt{r}} \quad (14)$$

where r is mirror radius. Value of constant A was estimated to be 3.5–4 for Hi Nicalon fibers [29,30].

Figure 15 shows that the flaw strengths derived from the mirror sizes correspond to the lower part of the strength cumulative distribution, calculated using Equation (6) for m = 6.8 and σ_0 = 61 MPa for Hi Nicalon filaments (Table 1). This may indicate that the weaker filaments broke in brittle mode during static fatigue. An alternative interpretation is that the size of the data set (21 data) was insufficient to represent the entire flaw strength population.

4.5.2. Fiber Overstressing

The presence of facies of brittle fracture under a stress = 525 MPa, which is quite low compared to the filament strengths (>800 MPa, Figure 15), suggests that the fracture of weaker filaments by slow crack growth was able to generate overstresses. Figure 16 compares the overstresses calculated using Equations (9) (assuming local load sharing) and (12) (assuming global load sharing), and the strengths of filaments derived from tensile tests on dry tow or from the fracture mirror sizes. In abscissa is the number of filaments broken according to the ascending order of strengths that were present right before a new failure of filaments. The curve of filament strengths was derived from the cumulative distribution function taking $N = N_0P$. The domain of interest is bounded by the theoretical failure limit of a dry tow in static fatigue under constant load and global load sharing. This limit corresponds to the critical filament, with strength characterized by probability α_t in the cumulative distribution function [21]: strength = 2000 MPa, α_t = 0.11 for Hi Nicalon fiber, N = 60. It is worth pointing out that theory showed that filament lifetime is commensurate with filament strength (Equation (5)), so that the lifetime of the tow is governed by the failure of weaker filaments.

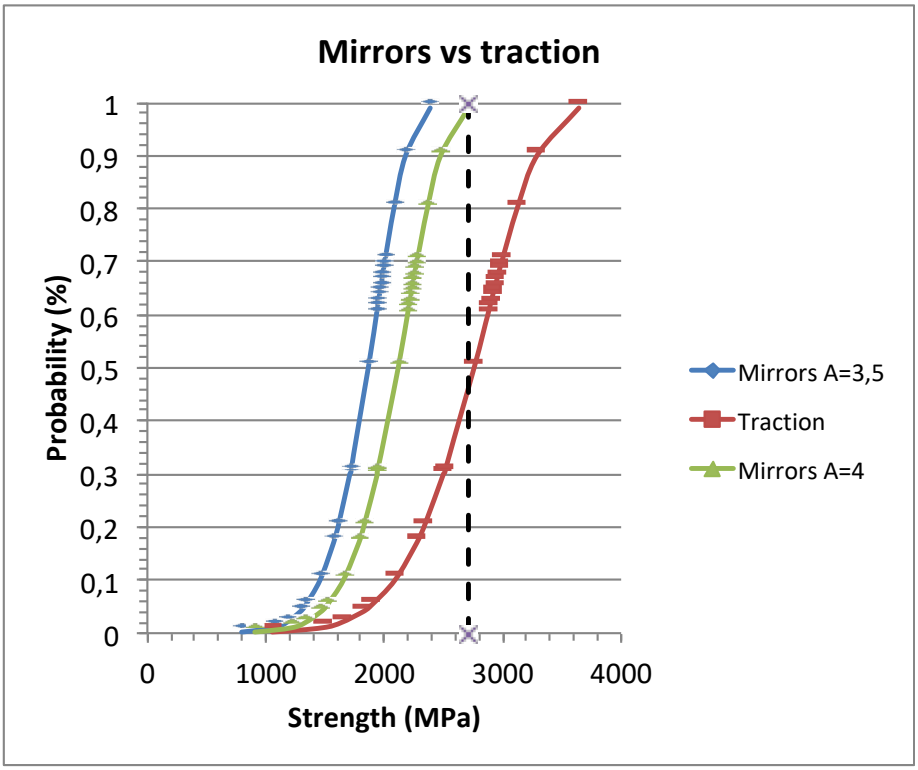

Figure 15. Comparison of flaw strengths derived from fracture mirror sizes and the cumulative distribution of filament strengths measured in tension. Probability for flaw strengths was estimated using the estimator $(i - 0.5)/n$, and i is the rank of the strength data in ascending order, n ($n = 21$) is the number of data.

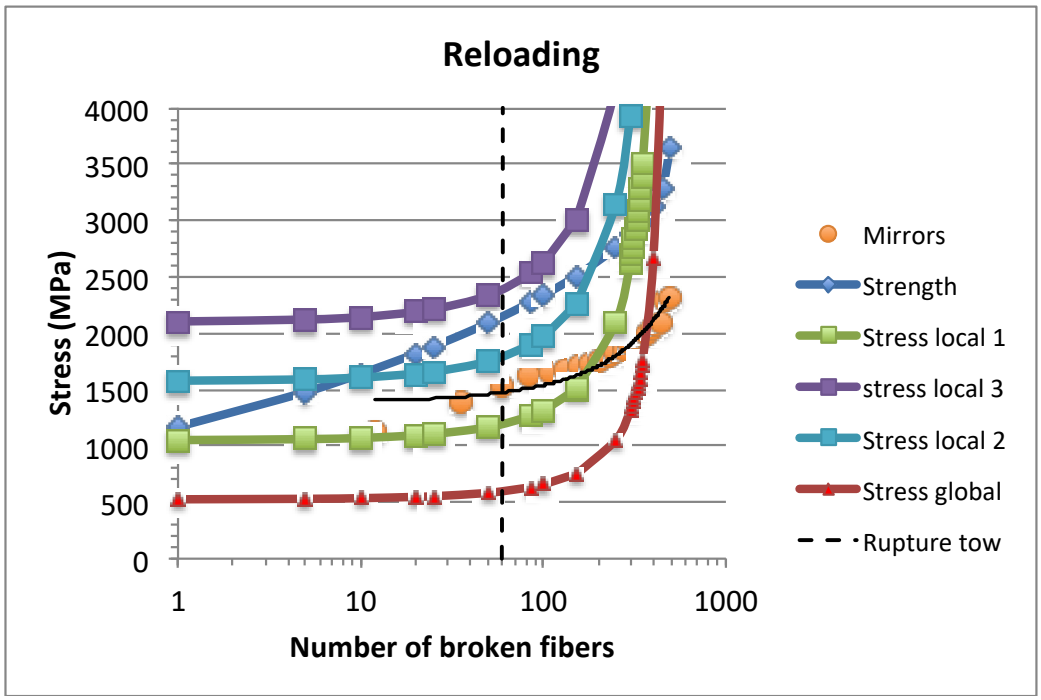

Figure 16. Reloading stresses computed using Equation (9) for global load sharing, and Equation (12) for local load sharing (for $j = 1, 2, 3$, and $k = 1$). Additionally shown are the filament strength cumulative distributions derived from the tensile behavior of the dry tow and from fracture mirror sizes.

In the domain of interest, the diagram shows that in conditions of global load sharing, the overstress remains below fiber strengths. By contrast, in conditions of local load sharing, the overstress can exceed filament strengths when at least two filaments fail simultaneously. Therefore, in these conditions filaments can fracture in brittle mode, as evidenced by the presence of fracture mirrors. It is worth noting that the flaw strengths derived from fracture mirrors correspond to the strength interval in the domain of interest (<2000 MPa). This suggests that this flaw strength interval was not underestimated, and that it was part of the lower part of the strength distribution derived from tensile tests, as mentioned above. This indicates the coherence of the results.

The brittle failure mode affects the current characteristic α_t of the critical filament, whose slow crack growth fracture triggers failure of the minicomposite. For instance, when $k = 1$ and $j = 3$, groups of four filaments fail, so that $N = 60$ is reached when 15 filaments have failed by slow crack growth. The corresponding value of α_t is 15/500 = 0.03. This result agrees with Figures 4–6.

5. Discussion

5.1. Mechanisms: The Contribution of the Oxide Scale on Filaments

The preponderant mechanism that governs lifetime of minicomposites is subcritical crack growth on weaker filaments, characterized by the low strength extreme of the cumulative distribution of reference strengths ($P < 0.11$ for Hi Nicalon). Oxidation is also responsible for the growth of an oxide layer on the surface of filaments. The thickness of the oxide scale increases with temperature. This was thin at 900 °C, and the filaments were not stuck to the matrix. At 1200 °C it was thicker, and more or less filled the gap in place of the removed interphases, but it was limited by the distance between the filament surface and matrix (Figure 13). It might be thicker at the surface of the filament located between the matrix crack lips, but crack opening is generally small (a few microns). The main identified contribution of oxide scale to lifetime was generating groups of filaments that were in direct contact, or were linked by the matrix when the interface gap was filled with oxide. The groups failed when their weaker filament failed from subcritical crack propagation.

It was inferred from the comparison of lifetimes of tows with that of the weakest single filament, that the phenomenon of slow crack growth was not slowed down by the growth of oxide scale when temperature increased. This conclusion agrees with earlier investigations of Hi Nicalon fiber oxidation [17]. Thus, it was reported that the analyses of Auger electron spectroscopy of Hi Nicalon filaments after static fatigue tests indicated that the oxygen diffusion is enhanced under load. The analyses also showed that the growth of the silica layer on the fiber surface does not cause filament fracture. Overestimated rupture times and stresses were predicted in [17] using the earlier mentioned Lara Curzio model [9,10]. Furthermore, it was shown in [19] that the reduction of filament diameter by oxidation at 1200 °C does not dictate rupture time of tows; experimental rupture times were significantly smaller than the times predicted from diameter decrease.

5.2. Stress–Rupture Time Diagram: Comparison of n and p Parameters

Results show that the empirical power law $t = A/\sigma^p$ does not properly fit the stress–rupture time diagrams, and that estimates of stress exponent p are significantly different from the intrinsic slow crack growth exponent n (Equations (2) and (5)). This difference was pointed out in an earlier paper on dry tows [20]. p was estimated from scattered data points of stress–rupture time diagrams for dry tows, and for minicomposites. The p estimates correspond to different values of strength/probability characteristics of the critical filaments, as a result of the collateral effects of high temperature oxidation of the filaments. The p and A parameters of the power law have no physical meaning because they do not reflect a single phenomenon, but instead the combination of a few erratic phenomena. They do not allow comparisons or predictions of stress–rupture time trends.

5.3. Rupture of Dry Tows and Minicomposites

Similarity between dry tows and minicomposites was observed for ultimate rupture under monotonous loading at room temperature, and static fatigue at high temperature when the filaments carry the load. In the first case, this is achieved after saturation of matrix cracking and complete fiber debonding. In the second case this is achieved in the presence of matrix cracks generated by the applied load and fiber debonding by consumption of the PyC interphase in the SiC–SiC minicomposite. In both cases, a critical filament triggers ultimate fracture. In the absence of structural effects, the critical filament is defined by a close form equation of probability in the cumulative filament strength distribution function, depending on either Weibull modulus (monotonous loading at room temperature) or Weibull modulus, and the slow crack growth K_I exponent (in static fatigue at high temperature). Structural effects include interactions of close filaments. At high temperature under constant load, interactions are enhanced by the growth of oxide scale on filaments. They are effective at lower temperatures on dry tows ($\leq$800 °C) when compared to minicomposites (1200 °C).

5.4. Variability of Critical Filament

The stress–rupture time data for dry tows and minicomposites show variation with the theory that was attributed to variability in the critical filament, which triggers catastrophic failure of specimens. The variability in the critical filament results from structural artifacts that are responsible for premature failures, such as the presence of groups of filaments that fail when a filament breaks by slow crack growth. The groups of filaments result from the fiber arrangement, fiber contacts, and fiber–matrix interactions that govern load transfers to neighboring fibers. They also depend on temperature, which activates growth of oxide scale on fibers, in place of removed pyrocarbon interphase. Whether the weak filaments are close to weak or strong filaments is also a factor that affects ultimate failure. Furthermore, the overstress magnitude depends on values of both j (the amount of simultaneous failures) and k (the number of reloaded neighboring filaments). Various combinations of j and k can occur, so that the value of overstress may vary during a static fatigue test, as well as from test to test. The occurrence of a combination and of a series of combinations is erratic. Variation of these factors cannot be addressed using close form equations. A parametric analysis can be performed for simulation purpose, but it does not allow the stress–rupture time behavior to be predicted. The bounds of stress–rupture time diagrams are provided by the lifetimes of the weakest and critical filaments, which are predicted using the theory of delayed failure of filaments.

5.5. Consequences: Guidelines to Improve Lifetime of Minicomposites

Under stresses below the proportional limit (about 70 MPa for SiC/SiC minicomposite), filaments are protected by the matrix from the environment. Lifetime is theoretically infinite.

Under higher stresses, owing to the presence of cracks, and associated fiber–matrix debonding, the lifetime of a minicomposite is dictated by fiber tow, and governed by the critical filament. The strengths of critical filaments are located at the low extreme of cumulative distribution function, bounded by $P = 1/N_0$ (N_0 = 500 for Hi-Nicalon) and $P = \alpha_t$ (Equation (10)). The following directions to improve minicomposite lifetime can be devised: (1) eliminate the weaker filaments (for instance by proof testing); (2) increase the strengths of filaments; (3) avoid filament clusters; and (4), owing to size effects on lifetime [30], optimize specimen size.

6. Conclusions

Filaments and tows govern the fatigue resistance of minicomposites at high temperatures under stresses above the proportional limit. Delayed failure of SiC–SiC minicomposites in static fatigue at temperatures $\leq$1200 °C is dictated by slow crack growth in filaments. An oxidizing environment activates this process. Temperature increase enhanced the collateral effects that reduced minicomposite resistance. These effects consist to fiber interactions

as a result of faulty fiber arrangement in the minicomposite, or of growth of oxide scale on fibers in place of the initial PyC interphase. They caused the failure of groups of filaments, and local load sharing.

Fracture of the critical filament dictated the ultimate failure of the minicomposites. Collateral effects affected the critical filament, characterized by strength/probability in the cumulative distribution function, which varied between $P = \alpha_t$ (Equation (10), $P = \alpha_t = 0.11$ for Hi Nicalon filaments), and $P = 1/500 = 0.002$ for the weakest filament. The stress–rupture time data showed significant scatter, resulting from variation of the critical filament. This trend cannot be predicted, but particular cases can be simulated.

The model of slow crack growth for filaments and tows was able to predict the bounds of the stress–rupture time diagrams of minicomposites at various temperatures. The contribution of multiple failures (groups of failures and local load sharing), associated with the failure of filaments from slow crack growth, was introduced for lifetime calculation at intermediate characteristics of critical filaments, in terms of probability in the cumulative distribution function.

Using the Weibull cumulative distribution function covered the intrinsic variability of lifetime resulting from flaw strength statistical distribution. The extrinsic variability caused by artifacts (failure of groups of filaments, fiber reloading by local sharing) cannot be described by a close form equation. Nevertheless, stress–rupture time values can be calculated for particular patterns.

Comparison of stress–rupture time diagrams for dry tows and minicomposites showed similarity in trends, but for dry tows the filament interactions were more significant, and lifetimes were shorter at higher temperatures. It appeared that the rate of slow crack growth was not slowed down by the presence of oxide scale on filaments.

Author Contributions: Conceptualization, J.L.; Formal analysis, J.L. and A.L.; Investigation, A.L.; Methodology, A.L.; Resources, A.L.; Supervision, J.L.; Writing—original draft, J.L. All authors have read and agreed to the published version of the manuscript.

Funding: This research received no external funding.

Conflicts of Interest: The authors declare no conflict of interest. The funders had no role in the design of the study; in the collection, analyses, or interpretation of data; in the writing of the manuscript, or in the decision to publish the results.

Appendix A

Filament Residual Strength

During time period t_F under constant stress σ on a filament, a crack propagates from initial flaw size a_i to length a_R, and the stress intensity factor increases from K_{Ii} to K_{IR}. The basic equation for time period t_F is derived from Equation (1):

$$t_F = \int_{ai}^{aR} \frac{da}{V} = \frac{2K_{IC}^n}{V^* Y^2 \sigma^2} \int_{K_{Ii}}^{K_{IR}} \frac{dK_I}{K_I^{n-1}} \tag{A1}$$

where Y is the flaw shape parameter ($Y = 2/\sqrt{\pi}$ for a penny-shaped crack).

Integrating gives:

$$t = \frac{2K_{IC}^n}{V^* Y^2 \sigma^2 (2-n)} \left[K_{IR}^{2-n} - K_{Ii}^{2-n} \right] \tag{A2}$$

From the following relations in Equation (5) between initial flaw size a_i, crack size a_R, applied stress σ, filament strengths σ_f, and relevant stress intensity factors, the relations in Equation (6) are derived:

$$K_{Ii} = \sigma Y \sqrt{a_i},\ K_{IR} = \sigma Y \sqrt{a_R},\ K_{IC} = \sigma_f Y \sqrt{a_i} = \sigma_R Y \sqrt{a_R} \tag{A3}$$

$$K_{Ii} = K_{IC} \frac{\sigma}{\sigma_f} \qquad K_{IR} = K_{IC} \frac{\sigma}{\sigma_R} \tag{A4}$$

where σ_f is the filament reference tensile strength in the absence of slow crack growth (it will be referred to as the reference strength) and σ_R is the residual strength.

Introducing relations (A3) and (A4) into Equation (A2) leads to the expression of residual strength σ_R:

$$\sigma_R^{n-2} = \sigma_f^{n-2} - t_F \frac{V^* \sigma^n Y^2 (n-2)}{2K_{IC}^2} \quad \text{(A5)}$$

References

1. Bansal, N.P.; Lamon, J. (Eds.) *Ceramic Matrix Composites: Materials, Modeling and Applications*; John Wiley and Sons, Inc.: Hoboken, NJ, USA, 2015; ISBN 9781118231166.
2. Lamon, J. CVI SiC/SiC Composites. In *Handbook of Ceramics and Glasses*; Bansal, N.P., Ed.; Kluwer Academic Publishers: New York, NY, USA, 2005; pp. 55–76.
3. Berger, M.; Hochet, N.; Bunsell, A.R. Small diameter SiC-based fibers. In *Fine Ceramic Fibers*; Bunsell, A.R., Berger, M.H., Eds.; Marcel Dekker: New York, NY, USA, 1999; p. 265.
4. Yun, H.M.; Di Carlo, J.A. Time/temperature-dependent tensile strength of SiC and Al2O3-based fibers. In *Ceramic Transactions, Advances in Ceramic-Matrix Composites II*; Bansal, N.P., Singh, J.P., Eds.; American Ceramic Society: Westerville, OH, USA, 1996; Volume 74, pp. 17–26.
5. Bunsell, A.R.; Piant, A. A review of the development of three generations of small diameter silicon carbide fibers. *J. Mater. Sci.* **2006**, *41*, 823–839. [CrossRef]
6. Shimoo, T.; Okamura, K.; Mutoh, W. Oxidation behavior and mechanical properties of low-oxygen SiC fibers prepared by vacuum heat-treatment of electron-beam-cured poly(carbosilane) precursor. *J. Mater. Sci.* **2003**, *38*, 1653–1660. [CrossRef]
7. Sha, J.J.; Park, J.S.; Hinoki, T.; Kohyama, A. Tensile properties and microstructure characterization of Hi-Nicalon SiC fibers after loading at high temperature. *Int. J. Fract.* **2006**, *142*, 1–8. [CrossRef]
8. DiCarlo, J.A.; Yun, H.M. Non-oxyde silicon carbide fibers. In *Handbook of Ceramics and Glasses*; Bansall, N., Ed.; Kluwer Academic Publishers: New York, NY, USA, 2005; pp. 33–52.
9. Lara-Curzio, E. Stress-rupture of Nicalon/SiC continuous fiber ceramic composites in air at 950 °C. *J. Am. Ceram. Soc.* **1997**, *80*, 3268–3272. [CrossRef]
10. Lara-Curzio, E. Analysis of oxidation-assisted stress-rupture of continuous fiber-reinforced ceramic matrix composites at intermediate temperatures. *Compos. Part A* **1999**, *30*, 549–554. [CrossRef]
11. Parthasarathy, T.A.; Przybyla, C.P.; Hay, R.S.; Cinibulk, M.K. Modeling Environmental Degradation of SiC-Based Fibers. *J. Am. Ceram. Soc.* **2016**, *99*, 1725–1734. [CrossRef]
12. DiCarlo, J.A.; Yun, H.M. Creep of ceramic fibers: Mechanisms, fundamentals and applications. In *Creep Deformation: Fundamentals and Applications*; Mishra, R.S., Earthman, J.C., Raj, S.V., Eds.; The Minerals, Metals and Materials Society: Warrendale, PA, USA, 2002; pp. 195–208.
13. DiCarlo, J.A.; Yun, H.M. Factors controlling stress-rupture of fiber reinforced ceramic composites. In Proceedings of the ICCM-12, Paris, France, 7–9 July 1999; p. 750.
14. Morscher, G.N. Tensile Stress Rupture of SiC_f/SiC_mMinicomposites with Carbon and Boron Nitride Interphases at Elevated Temperatures in Air. *J. Am. Ceram. Soc.* **1997**, *80*, 2029–2042. [CrossRef]
15. Morscher, G.N. Stress-rupture of new Tyranno Si-C-O-Zr fiber reinforced minicomposites. *Ceram. Eng. Sci. Proc.* **1999**, *20*, 379–386.
16. Gauthier, W.; Lamon, J. Delayed failure of Hi-Nicalon and Hi-Nicalon S multifilament tows and single filaments at intermediate temperatures (500–800 °C). *J. Am. Ceram. Soc.* **2009**, *92*, 702–709. [CrossRef]
17. Gauthier, W.; Lamon, J.; Pailler, R. Oxidation of silicon carbide fibers in air at intermediate temperature during static fatigue in air at intermediate temperatures. *J. Am. Ceram. Soc.* **2009**, *92*, 2067–2073. [CrossRef]
18. Loseille, O.; Lamon, J. Prediction of lifetime in static fatigue at high temperatures for ceramic matrix composites. *J. Adv. Mater. Res.* **2010**, *112*, 129–140. [CrossRef]
19. Laforet, A. Lifetime in Fatigue of Ceramic Matrix Composites at Temperatures between 800 °C and 1400 °C (French title: Durée en Fatigue des Composites à Matrice Céramique à des Températures Comprises Entre 800 °C et 1400 °C). Ph.D. Thesis, University of Bordeaux, Bordeaux, France, April 2009.
20. Lamon, J. Static fatigue of SiC multifilament tows at temperatures up to 1200 °C in air. *Ceramics* **2019**, *2*, 33. [CrossRef]
21. Lamon, J.; R'Mili, M. Damage and failure of SiC fiber tows during environment activated slow crack growth: Residual behavior and Strength-Probability-Time diagrams. *Acta Mater.* **2017**, *131*, 197–205. [CrossRef]
22. Lissart (Godin), N.; Lamon, J. Damage and failure in ceramic matrix minicomposites: Exprimental study and model. *Acta Mater.* **1997**, *45*, 1025–1044. [CrossRef]
23. Davidge, R.W.; McLaren, J.R.; Tappin, G. Strength-probability-time (SPT) relationships in ceramics. *J. Mater. Sci.* **1973**, *8*, 1699–1705. [CrossRef]
24. Charles, R.J.; Hillig, W.B. The kinetics of glass failure by stress corrosion. In Proceedings of the Symposium on Mechanical Strength of Glass and Ways of Improving It, Florence, Italy, 25–29 September 1961; Union Scientifique du Verre: Charleroi, Belgium, 1962.

25. Wiederhorn, S.M. Subcritical crack growth in ceramics. In *Fracture Mechanics of Ceramics*; Plenum Press: New York, NY, USA, 1974; Volume 2, pp. 613–646.
26. Coleman, B.D. Time dependence of mechanical breakdown in bundles of fibers. I. Constant Total Load. *J. Appl. Phys.* **1957**, *28*, 1058. [CrossRef]
27. Daniels, H.E. The statistical theory of the strength of bundles of threads I. *Proc. R. Soc.* **1945**, *A183*, 405–435.
28. International Standard ISO/22459. Fine Ceramics (Advanced Ceramics, Advanced Technical Ceramics)—Reinforcement of Ceramic Composites—Determination of Distribution of Tensile Strength and Tensile Strain to Failure of Filaments within a Multifilament Tow at Ambient Temperature 2020. Available online: https://www.iso.org/standard/73268.html (accessed on 28 February 2021).
29. Bertrand, S. Improvement of Lifetime of SiC/SiC Composites with Nanosized Multilayered Interphases. Ph.D. Thesis, University of Bordeaux, Bordeaux, France, September 1998.
30. Hurst, J.; Yun, H.M.; Gorican, D. A comparison of the mechanical properties of three polymer-derived small diameter SiC fibers. In *Advances in Ceramic-Matrix Composites III*; Bansal, N.P., Singh, J.P., Eds.; The American Ceramic Society: Columbus, OH, USA, 1996; Volume 74, pp. 3–15.